High-Q exterior whispering gallery modes in a metal-coated microresonator

Yun-Feng Xiao[1],* Chang-Ling Zou[2], Bei-Bei Li[1], Yan Li[1], Chun-Hua Dong[2], Zheng-Fu Han[2], and Qihuang Gong[1]†

[1] State Key Lab for Mesoscopic Physics, School of Physics,
Peking University, Beijing 100871, P. R. China and

[2] Key Lab of Quantum Information, University of Science and Technology of China, Hefei 230026, Anhui, P. R. China

(Dated: October 24, 2018)

We propose a kind of plasmonic whispering gallery modes highly localized on the exterior surface of a metal-coated microresonator. This exterior (EX) surface mode possesses high quality factors at room temperature, and can be efficiently excited by a tapered fiber. The EX mode can couple to an interior (IN) mode and this coupling produces a strong anti-crossing behavior, which not only allows conversion of IN to EX modes, but also forms a long-lived anti-symmetric mode. As a potential application, the EX mode could be used for a biosensor with a sensitivity high up to 500 nm per refraction index unit, a large figure of merit, and a wide detection range.

PACS numbers: 42.60.Da, 42.79.-e, 73.20.Mf

Optical whispering-gallery (WG) microresonators provide a powerful platform for various photonic applications ranging from low-threshold lasing to highly sensitive bio/chemical sensing [1]. They are also used for fundamental studies including cavity optomechanics [2], cavity quantum electrodynamics (QED) [3, 4] and quantum information science [5, 6] in the past few years. WG modes are dominantly confined in the high-refraction-index dielectric material, i.e., the inside of the cavity body. The other few energy of the WG mode is stored in the weak exterior evanescent field with a characteristic length of tens to hundreds of nanometers. The evanescent field is of importance because it offers the effective pathway to exchange the energy between the cavity mode and the external devices, i.e., the near-field coupling.

Furthermore, important applications of WG modes lie on the evanescent field since it determines the light-matter interaction strength. For instance, the resonant wavelength of the WG mode is sensitive to the refractive index change induced by the binding of biological/chemical molecules to the resonator surface. Thus, WG microresonators can be used for highly sensitive detection of single biological/chemical molecules, which attracts a strongly increasing attention very recently [7, 8]. Nevertheless, the detection sensitivity is strongly limited by the weak exterior evanescent field. In this Letter, we propose a new kind of WG modes of a metal-coated silica microcavity. Unlike the conventional WG modes distributing inside of the cavity body, the proposed new WG modes are concentrated in the exterior surface of the coated microcavity. Assisted by the propagating surface plasmon, these exterior (EX) modes show a high localization and reasonable high quality factors.

The geometry of the proposed metal-coated silica microcavity is shown in Fig. 1(a), where R and R' are the major and minor radii of the silica toroid, t represents the metal thickness. The boundary radius is defined as $R_b = R + R' + t$. At room temperature, the permittivities of silica and metal (here we choose silver as an example)
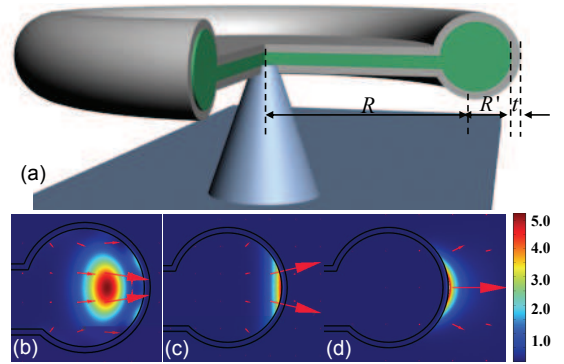

FIG. 1: (Color online) (a) Schematic illustration of a metal coated silica toroidal microcavity supported by a silicon pillar. (b)-(d) False-color representations of the squared transverse electric fields for optical, IN and EX plasmonic WG modes, respectively, where red arrows show the directions of the electric fields. In optical mode, a minor mode hybridization exists.

are $\epsilon_1 = 1.4457^2$ and $\epsilon_2 = -22.69 + 0.233i$ in the 680 nm band, respectively. The permittivity of the surrounding dielectric material is denoted as $\epsilon_3 = n_3^2$. In the following study, on one hand, we fix $R' = 1$ μm, ϵ_1 and ϵ_2, but vary the parameters R, t, and ϵ_3. On the other hand, since the EX mode has the great potential in biosensing, n_3 is set around 1.33 (the refraction index of water). To intuitively exhibit the EX modes, here we first resort to a full-vectorial eigenmode solver [9]. Figures 1b-1d show field intensity distributions $|E(\vec{r})|^2$ of three typical WG modes. The first is inside of silica, which is the conventional optical WG mode. The second is localized in the interior surface of the coating, and the similar interior (IN) plasmonic modes have been investigated in a metal-coated silica microdisk recently [10, 11]. The last is localized in the exterior surface of the coating, which is the focused scope of the present paper. In general, the EX modes can be tentatively identified by two parameters: the angular mode number l and the azimuthal mode number m. Due to the surface-plasmon property, they

are inherently quasi-TM and fundamental radial modes. In this Letter, we focus on the fundamental azimuthal modes, i.e., $m = l$.
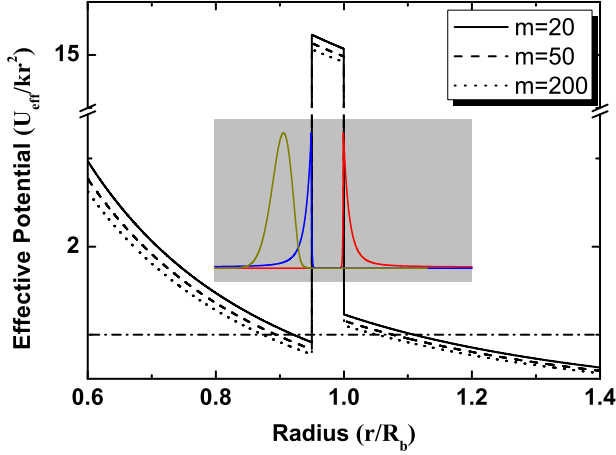

FIG. 2: (Color online) Effective potential function $U_{\text{eff}}(r)/kr^2$ for a layered 2D resonator with a silica core coated by a negative silver layer, where $k = 2\pi/\lambda$. The horizontal dash-dot line shows the normalized photon energy. The radial distributions of optical mode, IN and EX plasmonic modes are shown in yellow, blue, and red curves, respectively. Here $n_3 = 1.33$.

Before further investigating the EX mode numerically, we turn to theoretically analyze the confinement mechanism. Here a 2D model is adopted for simplification because there is no analytical solution to the toroid shaped resonator and the 2D model could be a good approximation as the EX mode is on the equatorial plane. It is obvious that both EX and IN modes are plasmonic modes which propagate along the metal-dielectric interface. Their energies are stored in the form of the collective oscillation of electrons in metal and evanescent wave in the surrounding dielectric. The effective potential approach [12] provides a good physical insight into many properties of the WG modes that appear as quasibound states of light, analogous to the circular Rydberg states of alkali atoms. Thus, in Fig. 2, we plot the effective potential of an EX mode of a layered 2D resonator (very similar results can be obtained for the IN plasmonic and conventional optical WG modes). It can be found that the negative permittivity of metal leads to a potential barrier inside the cavity. This configuration of the effective potential produces three kinds of WG modes: conventional optical mode, IN and EX plasmonic modes, corresponding to Figs. 1b, 1c and 1d.

To characterize EX modes in more detail, we now investigate the spatial distributions through the full-vectorial eigenmode solver. The mode energy fractions in the inner silica, metal nanolayer, and outer surrounding are denoted as $\eta_{1,2,3}$, respectively. By changing the metal thickness t, the curves in Fig. 3a illustrate the following points. (i) The EX mode has considerable dis-
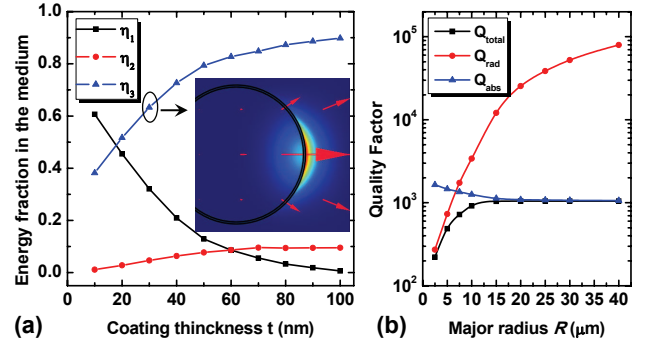

FIG. 3: (Color online) (a) Mode energy distribution fractions of an EX WG mode $\eta_{1,2,3}$ in silica, metal and surrounding medium, respectively. Here $R = 10$ μm and $n_3 = 1.33$. Inset: The mode distribution when $t = 30$ nm. (b) Total, radiation-related, and absorption-related quality factors, Q_{total}, Q_{rad}, and Q_{abs}, depending on the major radius R. Here $t = 100$ nm and $n_3 = 1.33$.

tributions in both the inner silica and outer medium in the case of a thin coating, for example, $\eta_1 = 0.60644$ and $\eta_3 = 0.38193$ when $t = 10$ nm; while the minor energy is in the coating nanolayer ($\eta_2 = 0.01163$). This phenomenon reflects the fact that the EX mode can tunnel to the inner through the potential barrier shown in Fig. 2. (ii) The fraction η_1 decreases quickly with increasing the coating thickness. In particular, η_1 approaches 0 for a large enough thickness (for example, $t = 100$ nm). (iii) As expected, more and more energy distributes in the exterior of the microcavity when the coating thickness increases. For example, η_3 reaches 90% at $t = 100$ nm. Qualitatively, the inset picture in Fig. 3a, with $t = 30$ nm, shows that the EX mode has invaded the interior silica. In addition, the EX mode is highly localized on the exterior surface of the coated cavity. The effective mode area is defined as $A_{\text{eff}} \equiv \int_A u(\vec{r}) dA / u(\vec{r})|_{\text{max}}$, where $u(\vec{r}) = \left[d\left(\omega\epsilon(\vec{r})\right)/d\omega \left|E(\vec{r})\right|^2 + \mu_0 \left|H(\vec{r})\right|^2 \right]/2$ gives the mode energy density, with the electric and magnetic fields $E(\vec{r})$ and $H(\vec{r})$, respectively, the dielectric permittivity $\epsilon(\vec{r})$ and the permeability of vacuum μ_0. A_{eff} is typically smaller than 0.1 μm^2 with the coating thickness t ranging from 10 to 100 nm, much smaller than the conventional optical WG mode with the same cavity size.

Quality factor of the mode, associated with the photon lifetime in the cavity, is one of the important parameters of an optical resonator. Here we not only provide the total quality factor Q_{total}, but also separately calculate the radiation and metal absorption related quality factors Q_{rad} and Q_{abs}, respectively, though these two contributions can not be separated experimentally. Thus it allows systemically studying of the different dissipation mechanisms of the EX mode. Here the loss caused by silica or water absorption has been omitted since it is much smaller than the silver absorption. As shown in Fig. 3b, Q_{rad} (by assuming pure real silver permittivity) increases

while Q_{abs} decreases with increasing the cavity major radius R. For Q_{rad}, it is reasonable since the large size will reduce the radiation loss; while for Q_{abs}, its decrease results from that more and more energy distributes in the metal layer. These two results can also be understood from Fig. 2. With increasing the cavity size (thus increasing the mode number m), the potential barrier is lowering, and the light has a larger penetration depth in the metal. Thus more energy will be confined in the metal, and this suppresses Q_{abs}. Moreover, the increasing energy in the metal results in a larger momentum of light. This makes the light more difficult to escape or couple to free space due to the momentum mismatching (i.e., reduce the radiation loss). It is easy to find that at a very large R, the total quality factor is limited by the metal absorption loss, i.e., $Q_{\mathrm{total}} \sim Q_{\mathrm{abs}}$; while for a small R, Q_{total} mainly depends on the radiation loss. The total quality factor reaches 1000 when the major radius is 10 μm, which is much larger than most plasmonic microcavities [13–17].
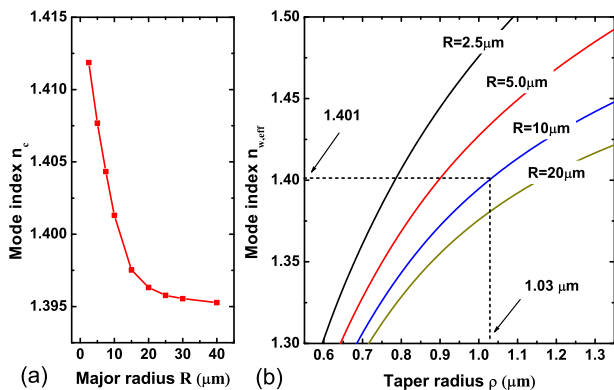

FIG. 4: (Color online) (a) EX WG mode index n_c for the different major radius. (b) Transformed mode index $n_{w,tr}$ of the straight fiber taper waveguide in the curved geometry of the cavity. Curves from left to right correspond to $R = 2.5, 5, 10, 20$ μm, where the taper is attached on the surface the coated microcavity. Here $t = 100$ nm and $n_3 = 1.33$.

The energy exchange (i.e., coupling) between an optical microcavity and an external device is of importance since it directly affects most applications. To realize an efficient coupling, there are two essential requirements: (i) sufficient spatial overlap of the cavity mode field and external device, (ii) phase matching condition between them. Here we propose that a tapered fiber waveguide with waist diameter 2ρ can implement such a near-field coupling [18]. For the requirement (i), the EX WG mode possesses an inherent advantage because the mode field dominantly distributes in the exterior of the cavity body. As a result, it allows building a very strong spatial overlap between the EX and waveguide modes. Here we consider that the waveguide is attached to the cavity to obtain the maximum coupling strength. For the requirement (ii), it is necessary to compare the cavity and

waveguide mode indexes n_c and n_w. The cavity mode index n_c of a specific eigenmode (angular mode number l, resonant wavelength λ) can be evaluated with respect to the cavity edge as $n_c = l\lambda/(2\pi R_b)$. As shown in Fig. 4a, n_c gradually decreases from 1.41187 to 1.39527 with increasing the cavity major radius R. This decrease is due to the choice of the cavity edge R_b. A rigorous calculation should consider the effective radius R_e, which is typically larger than R_b for EX modes. Nevertheless, the present n_c is still valid because both n_c and n_w are evaluated based on R_b.

It should be emphasized here that $n_c = n_w$ is not the exact phase matching condition because of the curved and straight geometries of the cavity and waveguide. As seen by the curved cavity, n_w has an effective mode index $n_{w,\mathrm{eff}} = n_w/\left(1 + \delta/3 + 2\delta^2/15 + O(\delta^3)\right)$ with $\delta = -\rho/R_b$ [19]. Thus, the exact phase matching condition should be $n_c = n_{w,\mathrm{eff}}$. Figure. 4b displays the effective waveguide mode index $n_{w,eff}$ depending on R and ρ. A thicker tapered waveguide will result in a larger mode index $n_{w,eff}$. As we can see from these curves, $n_{w,\mathrm{eff}}$ easily covers 1.3 to 1.5 for a micron-sized taper. For instance, when $R = 10$ μm, n_c is about 1.401. To achieve the phase matching condition, the taper radius can be around 1.03 μm, which is attainable with current technique.
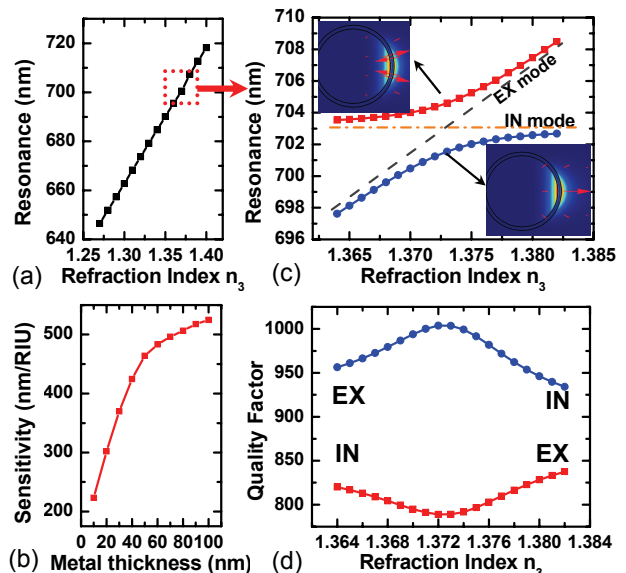

FIG. 5: (Color online) (a) Resonant wavelength of an EX mode vs. the refraction index n_3. Here $R = 10$ μm and $t = 100$ nm. (b) The sensitivity depending on the coating thickness. (c) Anti-crossing phenomenon of the resonant wavelengths when n_3 is around 1.37. As a guide the eye, black dash and orange dash-dot lines show the wavelengths of the uncoupled EX and IN WG modes, respectively. (d) The quality factors of the modes corresponding to (c). The curves are fitted with Eq. (1).

As mentioned above, the EX mode may be applied in highly sensitive biosensors. To demonstrate this po-

tential, Fig. 5a plots the resonant wavelength of a specific EX mode for different refraction index n_3 of the surrounding dielectric (this can simulate the binding of biological/chemical molecules to the resonator surface). It shows a highly linear increase with increasing n_3. By calculating the slope, we can obtain the sensitivity of the biosensing, defined as $S = d\lambda/dn_3$. Figure 5b shows that the sensitivity monotonously increases with the coating thickness. This result can be understood by considering the mode energy fraction η_3 in the surrounding dielectric (blue line in Fig. 3a). It can be found that the sensitivity of the EX mode-based sensor exceeds 500 nm/RIU (Refraction index unit). Furthermore, the overall figure of merit (FoM) defined by the ratio of the sensitivity and the resonance linewidth, is also studied. Since the EX mode has a high quality factor of 1000, the corresponding FoM reaches 700, exceeding (at least highly comparable to) the propagating surface plasmon [20] or the fiber Bragg grating [21] based biosensing.

It is interesting to note that a minor nonlinearity occurs when n_3 is around 1.37. To explicitly expose the underlying physics of the WG mode in this area, we further calculate the resonant wavelengths of the modes with a much smaller n_3 change (0.001). As shown in Fig. 5c, a clear anticrossing occurs where two energy eigenvalues come near to cross but then repel each other, similar to the strong interaction between a microcavity resonance mode and a two-level quantum dot. This is the signature of a strong coupling between the fundamental EX and IN WG modes, as depicted by the mode distribution in the insets of Fig. 5c. The strongest coupling occurs at $n_3 \approx 1.373$ where not only the two modes are spatially overlapped in the metal nanolayer but also their mode indexes are exactly matched. On the left side of this point, the red data points are the IN-like modes while the blue points represent the EX-like modes, and it is opposite on the right side. Remarkably, this anticrossing behavior, arising from the phase-matched interaction between the EX and IN modes, offers an efficient pathway to convert the IN mode to the EX mode. Furthermore, the quality factors of these two coupled modes are plotted in Fig. 5d. It shows a strong modulation by the coupling and forms a long-lived anti-symmetric mode (upper curve) due to the external coupling [22].

In general, this mode coupling can be described in terms of a 2×2 Hamiltonian matrix with eigen energies of the two modes E_1 and E_2, and the coupling terms $V_{1,2}$. Under the coupling, it forms two new eigen states (symmetric and asymmetric modes) with energies $E = (E_1 + E_2)/2 \pm \sqrt{(E_1 - E_2)^2/4 + V_1 V_2}$. Fitting with this theoretical description, we obtain the coupling strength $\sqrt{|V_1 V_2|} \sim 1$ THz (3.8 meV).

In summary, a new kind of WG modes is theoretically studied to be highly localized on the exterior surface of a metal-coated silica toroid microcavity. The EX WG modes possess a high quality factor up to one thousand at room temperature and can be efficiently excited by a tapered fiber. The coupling between IN and EX modes is also investigated. It is found that the coupling not only produces a strong anti-crossing, but also forms a long-lived anti-symmetric mode. Potentially, these EX modes are a widely useful advance beyond the IN modes described in Ref. [10], for instance, highly sensitive biosensors with a wide detection range.

* Electronic address: yfxiao@pku.edu.cn
† Electronic address: qhgong@pku.edu.cn

[1] For a review, see K. J. Vahala, Nature **424**, 839 (2003).
[2] For a review, see T. J. Kippenberg and K. J. Vahala, Optics Express **15**, 17172 (2007).
[3] T. Aoki *et al.*, Nature **443**, 671 (2006).
[4] Y.-S. Park, A. K. Cook, and H. Wang, Nano Lett. **6**, 2075 (2006).
[5] Y.-F. Xiao, Z.-F. Han, and G.-C. Guo, Physical Review A **73**, 052324 (2006).
[6] E. Waks and J. Vuckovic, Phys. Rev. Lett. **96**, 153601 (2006).
[7] F. Vollmer *et al.*, Appl. Phys. Lett. **80**, 4057 (2002).
[8] X. Fan *et al.*, Anal. Chim. Acta **620**, 8 (2008).
[9] M. Oxborrow, IEEE Trans. Microw. Theory Tech. **55**, 1209 (2007).
[10] B. Min, E. Ostby, V. Sorger, E. Ulin-Avila, L. Yang, X. Zhang, and K. Vahala, Nature **457**, 455 (2009).
[11] R. Perahia, T. P. Mayer Alegre, A. H. Safavi-Naeini, and O. Painter, Appl. Phys. Lett. **95**, 201114 (2009).
[12] B. R. Johnson, J. Opt. Soc. Am. A **10**, 343 (1993).
[13] S. I. Bozhevolnyi, V. S. Volkov, E. Devaux, J.-Y. Laluet, and T. W. Ebbesen, Nature **440**, 508 (2006).
[14] J.-C. Weeber, A. Bouhelier, G. Colas des Francs, L. Markey, and A. Dereux, Nano Lett. **7**, 1352 (2007).
[15] H. T. Miyazaki and Y. Kurokawa, Phys. Rev. Lett. **96**, 097401 (2006).
[16] H. Ditlbacher *et al.*, Phys. Rev. Lett. **95**, 257403 (2005).
[17] E. Jan R. Vesseur, F. Javier Garcia de Abajo,and A. Polman, Nano Lett. **9**, 3147 (2009).
[18] M. Cai, O. Painter, and K.J. Vahala, Phys. Rev. Lett. **85**, 74 (2000).
[19] D. R. Rowland and J. D. Love, IEE Proc. J. Optoelectron. **140**, 177 (1993).
[20] J. Homola. Surface Plasmon Resonance Based Sensors; Springer: Berlin, Germany, 2006.
[21] A. N. Chryssis *et al.*, IEEE Journal of Selected Topics in Quantum Electronics **11**, 864 (2005).
[22] Q. H. Song and H. Cao, Phys. Rev. Lett. **105**, 053902 (2010).